A&A 490, 555–570 (2008)
DOI: 10.1051/0004-6361:200810120

Astronomy & Astrophysics

HI holes and high-velocity clouds in the spiral galaxy NGC 6946

R. Boomsma[1], T. A. Oosterloo[3,1], F. Fraternali[2], J. M. van der Hulst[1], and R. Sancisi[1,4]

[1] Kapteyn Astronomical Institute, University of Groningen, PO Box 800, 9700 AV Groningen, The Netherlands
e-mail: oosterloo@astron.nl
[2] Department of Astronomy, University of Bologna, Bologna, Italy
[3] ASTRON, Netherlands Institute for Radio Astronomy, Dwingeloo, The Netherlands
[4] INAF-Osservatorio Astronomico di Bologna, Bologna, Italy

Received 4 May 2008 / Accepted 12 July 2008

ABSTRACT

We present a study of the distribution and kinematics of the neutral gas in the low-inclination Scd galaxy NGC 6946. The galaxy has been observed for 192 h at 21-cm with the Westerbork Synthesis Radio Telescope. These are among the deepest observations ever obtained for a nearby galaxy. We detect widespread high-velocity H I (up to about 100 km s^{-1}) and find 121 H I holes, most of which are located in the inner regions where the gas density and the star formation rate are higher. Much of the high-velocity gas appears to be related to star formation and to be, in some cases, associated with H I holes. The overall kinematics of the high-velocity gas is characterized by a slower rotation as compared with the regular disk rotation.
We conclude that the high-velocity gas in NGC 6946 is extra-planar and has the same properties as the gaseous halos observed in other spiral galaxies including the Milky Way. Stellar feedback (galactic fountain) is probably at the origin of most of the high-velocity gas and of the H I holes. There are also indications, especially in the outer regions, – an extended H I plume, velocity anomalies, sharp edges, and large-scale asymmmetries – pointing to tidal encounters and recent gas accretion.

Key words. galaxies: individual: NGC 6946 – galaxies: ISM – galaxies: halos – galaxies: structure

1. Introduction

Deep H I surveys of nearby spiral galaxies carried out in recent years have revealed the presence of cold extra-planar gas and have opened a new chapter in the study of the disk-halo connection. An extended, lagging H I halo has been discovered in the edge-on galaxy NGC 891 (Swaters et al. 1997; Oosterloo et al. 2007). Extra-planar gas with similar properties has also been detected in a number of nearby spirals (see a review by Sancisi et al. 2008). Some of these (e.g. NGC 2403, Schaap et al. 2000; Fraternali et al. 2001) are not edge-on, and the presence of extra-planar H I has been inferred from its anomalous velocities. In the Milky Way, halo gas components are the well-known Intermediate-Velocity Clouds (IVCs) and, as conclusively shown by recent distance determinations (Wakker et al. 2007, 2008), also the High-Velocity Clouds (HVCs) (Wakker & van Woerden 1997).

The origin of the halo gas is still an open question. One of the mechanisms proposed is the so called Galactic Fountain (Shapiro & Field 1976; Bregman 1980) according to which gas, heated by stars and supernovae, leaves the disk and moves via chimneys in the vertical direction to fall back, eventually, onto the disk. There is also evidence, however, that part of the extra-planar gas must be infall from intergalactic space (Sancisi et al. 2008). It is likely, for example, that the Galactic HVCs, because of their low metallicity, are such accreted gas (van Woerden & Wakker 2004).

Most of the observations which have revealed the presence of extra-planar gas have been carried out for spiral galaxies viewed edge-on or highly inclined. Naturally, they have been used to study the vertical extent of the extra-planar H I and its rotation. A more "face-on" view is required to investigate the gas motion perpendicular to the plane, to detect high-velocity gas and to study its possible connections with structures in the disk, such as spiral arms, H I holes, star clusters, and H II regions.

For this purpose we have carried out a very sensitive H I survey with the Westerbork Synthesis Radio Telescope (WSRT) of the nearby spiral galaxy NGC 6946. This is a Scd galaxy seen at low inclination showing high-level star formation activity (Degioia-Eastwood et al. 1984). The bright optical disk ($R < R_{25}$) shows many large H II complexes. Some H II regions are also present in the outer arms (Ferguson et al. 1998). Furthermore, there is an extended disk of diffuse H α and X-ray emission (Schlegel et al. 2003).

Over the last 30 years, NGC 6946 has been observed several times in the 21-cm line. Rogstad et al. (1973) made the first synthesis observation at the Owens Valley Radio Observatory. Their H I map already showed a gas disk that extends well beyond the optical image and deviations from circular rotation could be seen in their velocity field despite the low resolution of 2′. Tacconi & Young (1986) confirmed these results with their 40″ data from the Very Large Array. Carignan et al. (1990) and Boulanger & Viallefond (1992) made a more detailed study of the kinematics and the distribution of the H I in NGC 6946 using the WSRT. They were the first to report the presence of holes in the H I distribution. In addition, they reported the detection of a diffuse fast gas component and of a few isolated high-velocity H I clouds. Kamphuis & Sancisi (1993) studied the widespread high-velocity H I and found that this is predominantly located in the direction of the bright optical disk suggesting a link with stellar winds and supernovae (i.e. a galactic fountain). Kamphuis (1993) also made the first detailed study of H I holes in this galaxy.

Table 1. General information on NGC 6946.

Type		SAB(rs)cd	1
Distance		6 Mpc	2
Position of nucleus	α(2000)	$20^h34^m52.3^s$	3
	δ(2000)	$60°09'14''$	
Kinematical centre	α(2000)	$20^h34^m52.36 \pm 0.13^s$	5
	δ(2000)	$60°09'13 \pm 2''$	
Holmberg radius		7.8′	4
$^aD_{25}$		11.2′	4
disk scalelength		1.9′	4
Position angle		242°	5
Inclination angle		$38 \pm 2°$	5
V_{sys}		43 ± 3 km s^{-1}	5
M_B		-21.38	4
L_B		$5.3 \times 10^{10} L_\odot$	4
H I mass		$(6.7 \pm 0.1) \times 10^9$ $M_\odot$	5
21-cm Flux		788 ± 12 Jy km s^{-1}	5
Conversion 1′		1.75 kpc	

Notes – [a] Diameter at the 25 B mag arcsec^{-2}. [1] de Vaucouleurs et al. (1976). [2] Karachentsev et al. (2000). [3] van Dyk et al. (1994). [4] Carignan et al. (1990). [5] This study.

Table 2. Observing parameters.

Date of observations		Dec. 2001–Jun. 2002
Total observing time		16×12 h
Observed baselines		36–2772 m, step: 18 m
Field centre	α(2000)	$20^h34^m52.3^s$
	δ(2000)	$60°09'14''$
Heliocentric velocity of central channel		48 km s^{-1}
Total bandwidth		5 and 10 MHz[a]
FWHM of primary beam		36′
Calibration sources		3C 286, 3C 48, 3C 147
Radii of first grating ring ($\alpha \times \delta$)		$40.4' \times 47.1'$
Number of antennas		14
Number of channels		512 and 1024[a]
Channel separation		2.1 km s^{-1}
FWHM velocity resolution		4.2 km s^{-1}
Frequency taper		Hanning
FWHM of synthesised beam		$12'' \times 14''$
r.m.s noise per channel		0.2 mJy (beam area)$^{-1}$
Conversion factor T_B(K)/S(mJy)		3.6

Note – [a] The first 8 observations have been done with 512 channels and 5 MHz bandwidth, the rest has been observed with 1024 channels and 10 MHz bandwidth.

Catalogues of H I shells have been compiled for the gas-rich galaxies in the Local Group, such as M 31 (Brinks & Bajaja 1986), M 33 (Deul & den Hartog 1990), the LMC (Kim et al. 1999) and SMC (Stanimirovic et al. 1999). Many H I holes have been detected in galaxies in neighbouring groups: Ho II (Puche et al. 1992), NGC 2403 (Thilker et al. 1998), IC 2574 (Walter & Brinks 1999), M 101 (van der Hulst & Sancisi 1988; Kamphuis 1993), and IC 10 (Wilcots & Miller 1998). The shells and holes are commonly thought to have been produced by clustered supernova explosions and stellar winds (Tomisaka & Ikeuchi 1986; McCray & Kafatos 1987; Mac Low & McCray 1988; Tenorio-Tagle & Bodenheimer 1988). Simulations show that these are energetic enough to form kpc-size bubbles and chimneys (see e.g. de Avillez & Berry 2001), which would appear as holes in the H I distribution, when observed in an external galaxy.

Here, we report the main results of a new, deep H I study of NGC 6946 with the WSRT. In particular, we draw attention to the presence of a large number of H I holes (Sect. 3.3) and of gas complexes with anomalous velocities (Sect. 3.4). We discuss the role of star formation and environment in the formation of these features (Sect. 4).

2. Observations and data reduction

We observed NGC 6946 (Table 1) with the upgraded WSRT, which has cooled frontends on all 14 telescopes. Sixteen 12-h observations were made between December 15, 2001 and June 7, 2002. We used the WSRT 36, 54, 72 and 90 m configurations to achieve a uniform *uv*-coverage. Each 12-h observation was preceded by a short observation of 3C286 and followed by a short observation of 3C 48 or 3C 147 for calibration purposes.

The *uv*-data reduction was performed with the MIRIAD package (Sault et al. 1995). We used as bandpass an average of the calibration observation before and after each 12-h run. In addition, the data were Hanning smoothed. The continuum has been subtracted by interpolating it with a 2nd-order polynomial omitting the channels with H I line emission. In order to improve the quality of the data we used self-calibration on the continuum in addition to the cross-calibration, and corrected residual phase errors using an iterative procedure. The first step was to form a model of the sky brightness distribution of the continuum emission using CLEAN components. With that model, the phase errors were corrected. After this first improvement of the calibration, a better sky model could be defined for the next iteration.

The data were Fourier-transformed with a robustness weighting of 0 (Briggs 1995). For the deconvolution of the data at the highest resolution, the multi-resolution clean (MRC) algorithm (Wakker & Schwarz 1988) was used within the GIPSY package (van der Hulst et al. 1992; Vogelaar & Terlouw 2001). This was necessary because of the large extent of the H I emission in each channel. The MRC algorithm was able to produce channel maps with a flat noise level. The resolution of the maps is $12'' \times 14''$ and the r.m.s. noise per channel is 0.22 mJy beam^{-1}. The velocity resolution is 4.2 km s^{-1}.

We also constructed low-resolution sets of channel maps to optimise the signal-to-noise ratio for extended emission. These sets were CLEANed in MIRIAD using the Clark algorithm. The resulting clean beams for the low-resolution data sets are $20.7'' \times 23.4''$ and $63.6'' \times 65.6''$. The noise level per channel for the $\sim 22''$ resolution set is 0.34 mJy beam^{-1} and for the $\sim 65''$ data cube 0.5 mJy beam^{-1}. The observational parameters are listed in Table 2.

3. Results

3.1. H I distribution

Figure 1 shows the total H I map of NGC 6946 compared to an optical image from the Digitized Sky Survey (same scale). This H I map was constructed from the high-resolution data cube using $64''$-resolution masks to define the area of the emission in each channel before adding them to produce the total H I map.

As seen in many spiral galaxies, the H I disk is much more extended than the bright optical disk. The inner gas disk shows the same pattern of filamentary spiral-arm structure as the optical. Outwards, the spiral arms become more pronounced. At least three spiral arms can be traced well. The northern arm is the most gas rich. It is more open and there is a high arm-interarm contrast. The inner H I disk shows a sharp edge on the side of the northern spiral arm. All outer spiral arms bifurcate half way, giving the outer edge a frayed appearance with many short spiral fragments (Fig. 2, left panel), except for the south-western edge.

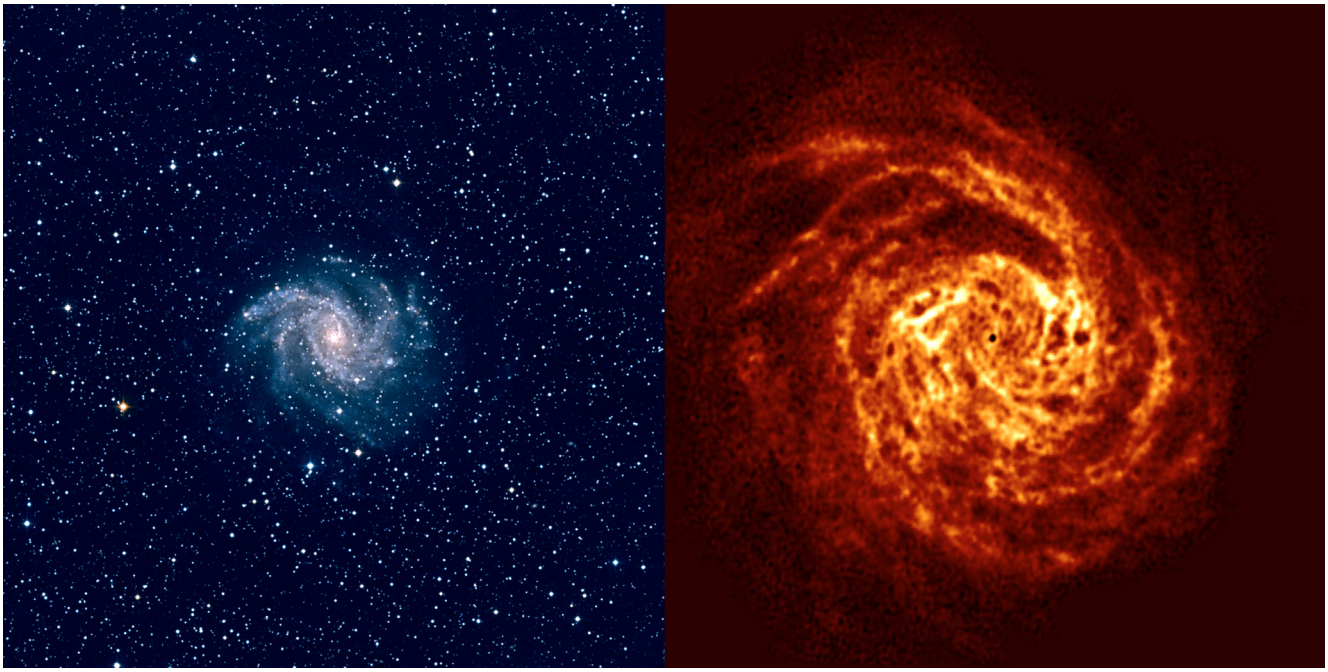

Fig. 1. *The left panel* is a colour composite of the Digitized Sky Survey plates. The *right panel* is the deep (192 h integration) H I map on the same scale as the optical. Column densities range from 6×10^{19} cm^{-2} to 3.7×10^{21} cm^{-2}. The H I in the centre is seen in absorption against the bright core, producing a black spot on the H I map.

The outer arms also contain stars as shown by Ferguson et al. (1998, see also Fig. 10 in Sancisi et al. 2008).

Also visible in Figs. 1 and in Fig. 2 is a prominent H I absorption in the centre (the black and the white dot respectively). This absorption is due to H I seen against the bright radio continuum nuclear source. In Fig. 2 (left panel) a minor bar (position angle $\sim -10°$) and the inner spiral arms appear symmetric with respect to the optical and radio nucleus.

In the outer parts the H I disk is asymmetric, i.e. more extended toward the south-eastern direction with respect to the bright optical disk (R_{25}, which is indicated by the ellipse in Fig. 2, see also Fig. 17). Despite this lopsidedness, the outer spiral pattern of NGC 6946 is quite symmetric. If we rotate the galaxy image by 180° and shift it by about 1′ to the south-south-east, then the northern and southern spiral arm fall perfectly on top of each other.

Figure 3 shows the global H I profile for NGC 6946 and for two companion galaxies (see Sect. 4.4). The positions of the latter with respect to NGC 6946 can be seen in Fig. 17. The integrated H I flux of NGC 6946 is 788 Jy km s^{-1}. If we use the distance of 6 Mpc as determined by Karachentsev et al. (2000), we obtain a total H I mass of 6.7×10^9 $M_\odot$. This is the same as the H I mass found by Carignan et al. (1990) (after converting their mass to our adopted distance) with the WSRT, using additional short-spacing measurements. Our results are consistent with those of single dish measurements ($8 \times 10^9 \pm 20\%$ $M_\odot$ according to Gordon et al. 1968) indicating that we are not missing any flux in our measurements. Rogstad et al. (1973) report a similar value of 7.4×10^9 $M_\odot$.

3.2. Large-scale kinematics

Some of the velocity channels (at negative velocities) are affected by foreground emission from H I in our galaxy. This foreground emission could, however, be removed almost completely, because of the difference in angular scale compared with the H I structures in NGC 6946. A striking feature of the H I line profiles of this galaxy is the presence, already noticed by Boulanger & Viallefond (1992) and by Kamphuis & Sancisi (1993), of extended velocity wings at low emission levels, due to gas at anomalous velocity with respect to the disk's rotation. To determine the velocity of the peaks and obtain the velocity field of NGC 6946, we fitted a Gaussian to the upper part (above 25%) of each profile, discarding the low intensity, broadened part. We included a 3rd-order Hermite polynomial in the fit to account for asymmetries in the profiles. For many profiles a fit to the whole profile with a single Gaussian without Hermite polynomials gave the same result; in regions with broad, asymmetric profiles the difference between the two fits was around 5 km s^{-1}. The uncertainty in the velocity field increases in the outer regions because of the lower signal-to-noise ratio. The resulting velocity field at 22″ resolution is shown superposed on the H I density distribution in Fig. 2.

Although NGC 6946 has a fairly low inclination (inclination angle 38°), differential rotation clearly shows up and dominates the overall kinematics of the galaxy. NGC 6946 appears to be a regularly rotating galaxy. There are no apparent large distortions within the optical radius (marked by the ellipse in Fig. 2), except some small-scale wiggles. Some of the wiggles in the inner regions follow the structure of the H I spiral arms and can probably be attributed to streaming motions along the arms. Their amplitude is of the order of 15 km s^{-1} (corrected for inclination) if the motions are in the plane of the disk.

In the outer parts the velocity field becomes more disturbed. On the northern side the iso-velocity contours are bent toward the approaching side (NE) over a large area. The sharpest gradient in the velocity field coincides with the middle of the northern spiral arm (Fig. 2). Further out to the north-west the contours bend back to higher velocities. This pattern continues over the whole west side of the disk and may be related to the plume of H I on the north-western side (see Sect. 4.4).

The most prominent disturbance in the velocity field of the outer disk is seen in the southern side. Close to the southern

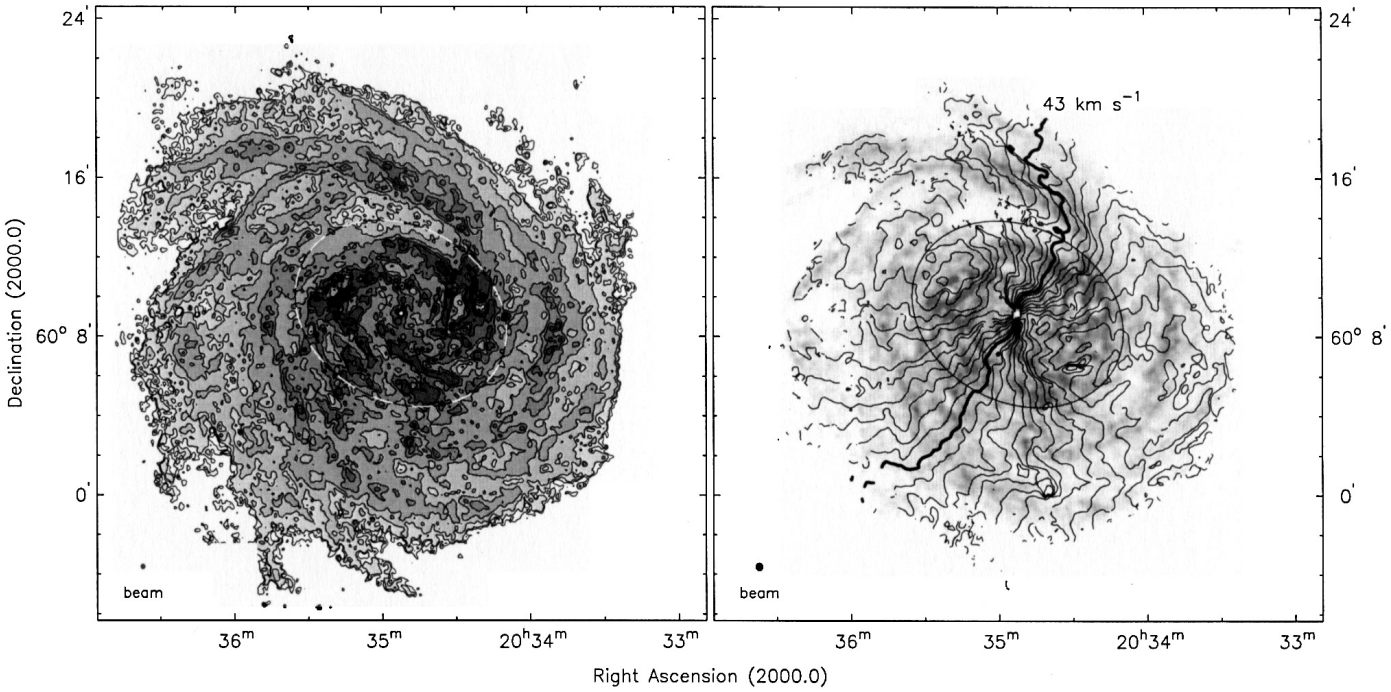

Fig. 2. *Left panel*: total H I distribution. The contour values are 0.6, 1, 2, 4, 8, 12, 16, 24, and 32×10^{20} cm^{-2}. The ellipse (dashed) indicates the bright optical disk (R_{25}). The white dot in the centre is due to absorption against the radio continuum source . The beam (12″ × 14″) is shown in the bottom left corner. *Right panel*: the velocity field at 22″ resolution plotted on top of the 13″ resolution total H I distribution (greyscale). The beam is shown in the lower left corner. The lines are separated by 10 km s^{-1} running from −70 to 150 km s^{-1}(NE approaching). The thick line shows the systemic velocity. The ellipse indicates the size and orientation of the bright optical disk (≈R_{25}).

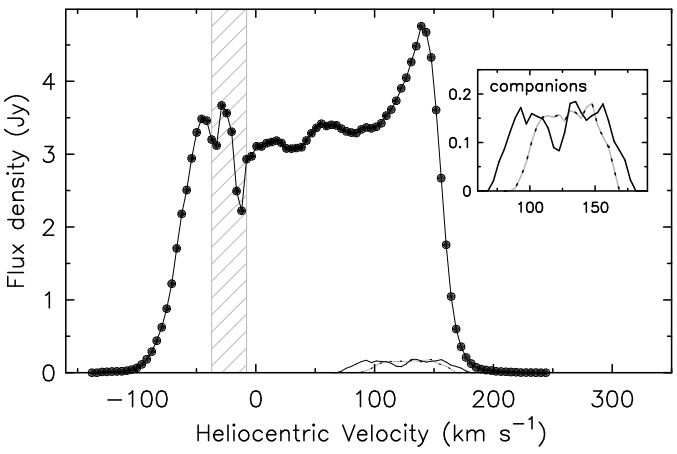

Fig. 3. Global H I profile of NGC 6946 and the two companions. The shaded band indicates the channels which are strongly affected by Galactic foreground emission. The inset shows a blow-up version of the profiles of the companions. The black line is the profile for UGC 11583, the dashed grey-black line for L 149.

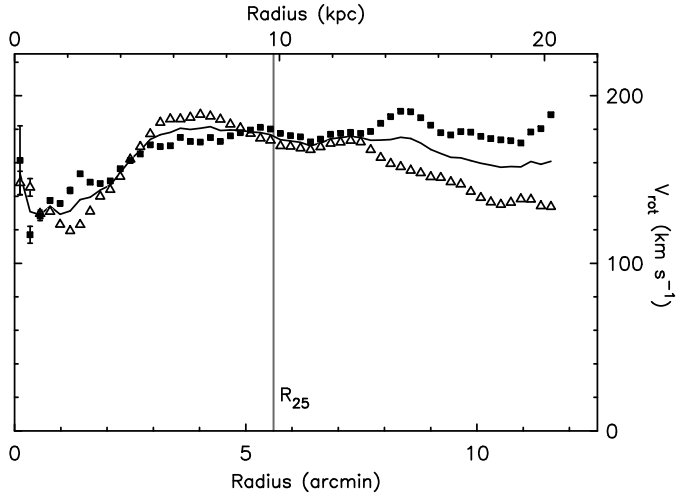

Fig. 4. The rotation curve for the receding side (filled squares) and the approaching side (open triangles) separately. The error bars show the formal errors from the fit, but they are generally very small. The line shows the fit to the whole velocity field. The vertical grey line indicates the optical radius R_{25}.

spiral arm, the wiggles are very large: the velocities drop by about 40 km s^{-1} (see Fig. 2 and Sect. 3.3).

3.2.1. Rotation curve

We performed a tilted-ring fitting of the velocity field in Fig. 2 following the scheme described by Begeman (1989). A similar analysis for NGC 6946 has been done before by Carignan et al. (1990). We iteratively improved the fit by fixing the parameters one by one starting with the centre of the rings. The kinematic centre coincides with the nucleus within the uncertainties. V_{sys} is constant out to a radius of 12.5 kpc and increases at larger radii. This behaviour has been observed in other galaxies and interpreted as a possible offset between the inner disk and the dark matter halo (Battaglia et al. 2006). We took the average of the inner disk, which is 43 ± 1 km s^{-1}. This differs slightly from the V_{sys} that we derive from the global profile: 47 ± 2 km s^{-1}. Except for a dip at R = 11 kpc, which seems related to the outer H I arm, the fitted inclination angle appears approximately constant (Boomsma 2007). We adopt a constant value of i = 38 ± 2°.

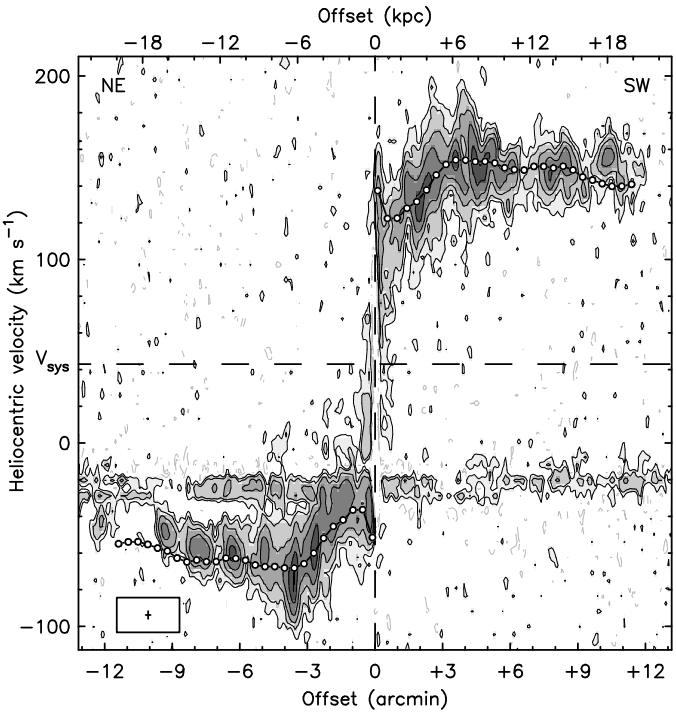

Fig. 5. The rotation curve of NGC 6946 plotted on a *p-v* slice along the major axis.

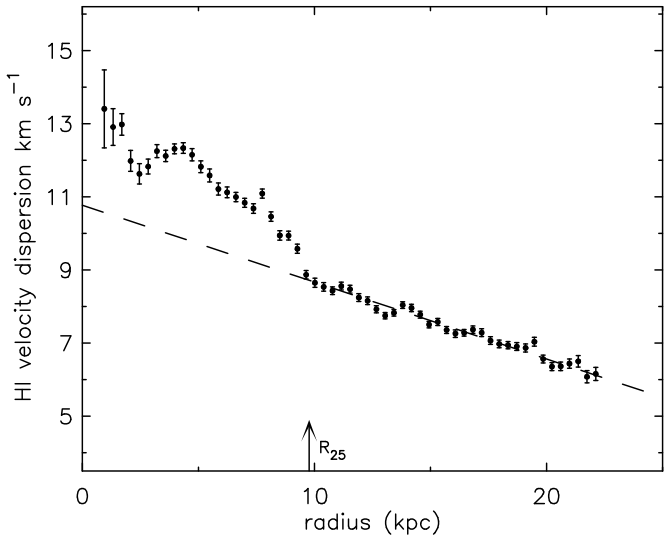

Fig. 6. Radial profile of the H I velocity dispersion in NGC 6946 at 13″ resolution. The dispersions are corrected for instrumental broadening. The dashed line shows the approximate linear trend of the dispersion in the outer disk extrapolated to smaller radii. R_{25} is indicated by the arrow.

The rotation curves, derived separately for the two sides, are shown in Fig. 4. For radii out to ∼13 kpc, they are similar. In the outer parts, the differences become large. These differences are also seen in Fig. 5, where we show the average rotation curve overlaid on a position-velocity plot along the major axis of the galaxy. The rotation curve is determined out to about 21 kpc ($\approx 2R_{25}$).

In Fig. 4 we show the formal errors of the fit. The actual uncertainties can be estimated using the difference in rotation velocity between the mean rotation curve and the curves on either sides (cf. Swaters 1999). This procedure leads to errors of 3–4 km s^{-1} in the inner parts rising to about 10 km s^{-1} beyond 13 kpc. Furthermore, one should include the 2° uncertainty in the inclination, which introduces another systematic 5% uncertainty in the rotation velocities.

The signal-to-noise in the outer regions is better at 64″ resolution. On the receding side (west), there is, however, a sharp edge and the rotation curve cannot be determined out to radii larger than ∼21 kpc. On the approaching side the rotation curve continues declining out to the last measured point at about 28 kpc. Also the fit of the velocity field at 64″ resolution gives no indications for a change in the inclination at large radii.

3.2.2. Velocity dispersion of the cold disk

As mentioned earlier in this section, most H I velocity profiles show a nearly Gaussian shape. Figure 6 shows the azimutally averaged values of the velocity dispersion (see also Boulanger & Viallefond 1992). This decreases with radius from about 13 km s^{-1} in the centre to about 6 km s^{-1} in the outskirts. Around R_{25} there is a dropoff followed by a remarkable linear decrease from 9 km s^{-1} to 6 km s^{-1}. The run of velocity dispersions in the inner regions is much less regular than in the outer regions, with *bumps* at R = 2 and 4 kpc. The general decrease from the inner to the outer parts is similar to those found for M 101 and NGC 628 (see Kamphuis, Ph.D. Thesis 1993).

3.3. H I holes

Expanding shells and H I cavities present a clearly recognisable pattern in velocity-space and are, therefore, easier to identify on position-velocity (*p-v*) maps than on channel maps. A disadvantage of only looking in velocity-space is that one can mistake interarm regions for shells or holes. Interarm regions are, on the other hand, easily recognisable in channel maps, so the safest procedure is to identify shells inspecting the full 3-D data cube.

The hole-type identification scheme is the same as adopted by Brinks & Bajaja (1986). There are three types of holes: type 1 is an open hole, without expanding shell, and in a *p-v* diagram it appears as a density gap. Type 2 is characterised by a velocity shift in the *p-v* diagram. In type 3 holes there is a clear splitting of the line profiles into two components. See also Fig. 10 in Deul & den Hartog (1990) for a clear illustration of the three types.

In the central parts of NGC 6946 we may miss some holes because of the strong shear. On the north-eastern side it is more difficult to identify the holes because of Galactic foreground emission.

The holes are shown in Fig. 7 as ellipses indicating size and orientation. Figure 8 shows examples of H I holes compared to the H α emission in the same regions (see Sect. 4.1).

3.3.1. Distribution of H I holes

We find 121 H I holes distributed over the whole disk, but mainly in regions with high H I column density (Fig. 7). As compared to the starlight, the distribution of the holes appears to be more extended: many are found outside R_{25} where the stellar density is low (Fig. 9, bottom right). Furthermore, the holes are asymmetrically distributed as compared to the bright optical disk, although some asymmetry is also seen in the low level stellar brightness. Optical emission (bright in the inner-disk, faint in the outer-disk) is seen in the direction of nearly every hole.

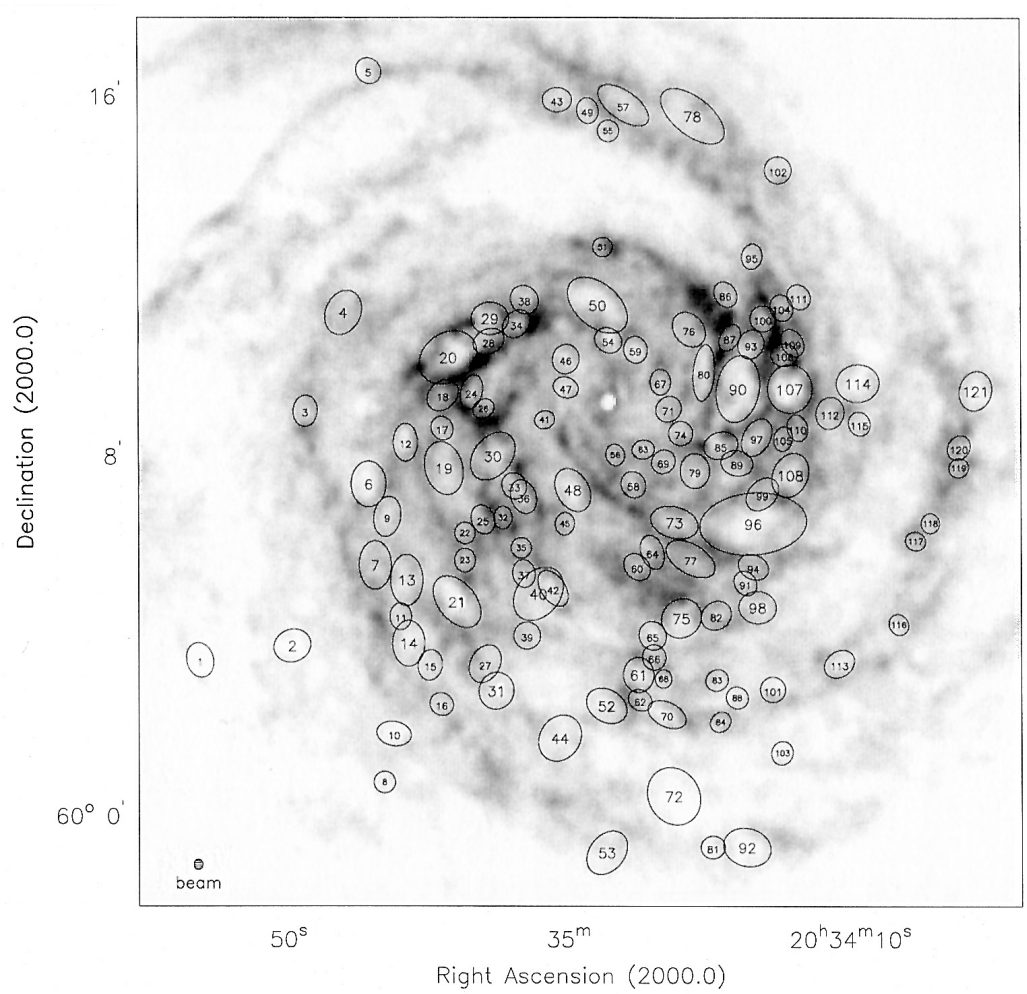

Fig. 7. The H I holes plotted on top of the total H I map of NGC 6946. The sizes and orientations are indicated by the ellipses. The white spot in the centre is not an H I hole, but is the result of H I absorption against the bright radio continuum nucleus. The resolution is shown by the shaded ellipse in the bottom left corner.

The radial number-distribution of the holes (Fig. 10a) shows a broad peak around 10 kpc, which is about R_{25}. Perhaps, a better representation of the importance of the holes is given by the covering factor shown in Fig. 11. The peak in the coverage appears at smaller radii than the number distribution and shows that the holes are most dominant within the bright optical disk. The covering factor drops sharply toward the smallest radii. The average H I column density also drops sharply in the inner regions, which probably prevents the detection of holes. The lack of inner holes may also be caused by the strong shear, which shortens their lifetimes. At large radii, where the average H I column density is below about 5×10^{20} cm^{-2} the covering factor drops again. The radial distribution of star formation (Hα brightness) in the disk shows the same trend as the holes, suggesting that they are related.

3.3.2. Hole sizes

There seems to be no correlation between the diameters of the holes and their distance from the centre, except that no holes larger than 1 kpc exist in the inner 4 kpc. The latter may be related to the galactic shear as suggested earlier.

For the holes larger than 1 kpc the size distribution is approximately exponential (Fig. 10b). For smaller sizes, the numbers drop sharply. Even though the highest spatial resolution of the present data is 390 pc, the smallest hole we find has a diameter of 766 pc. If we extrapolate the exponential size distribution down to the resolution of the data, we miss about 250 holes. This would mean that we have only detected 1/3rd of the holes.

The average diameter of the holes is 1.2 kpc, which is large compared to the typical H I disk scale heights for a galaxy like NGC 6946. If we assume an average scale height h of 200 pc even the smallest hole in our catalogue of 766 pc size would reach about 2 scale heights above the midplane. There, the gas density is about 10% of the midplane density. This would imply that all holes that we detect must have broken out of the thin disk into the halo. Once broken out, a bubble looses pressure and the interior is blown into the halo. Without the pressure, further expansion of the bubble in the plane would seem to be difficult. Nevertheless, we detect holes with sizes up to 3 kpc. This may suggest that the expansion continues effectively in the plane. Some of the largest holes may also be a blend of a number of smaller ones.

3.3.3. Missing H I

We estimated the missing H I mass from the holes by assuming that the initial (pre-superbubble) column density at the location

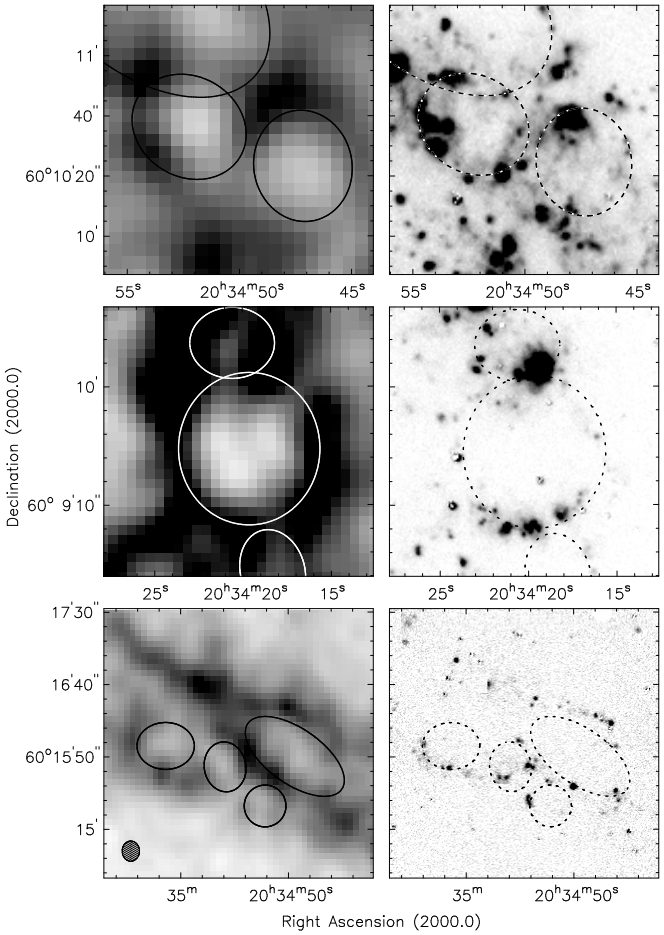

Fig. 8. Example of H I holes and associated H II regions. *From top to bottom* the galactocentric distance increases. *The left panels* show the total H I density distribution around the holes. The ellipses show the derived size and orientation of the H I holes. The beam is shown in the *bottom left corner*. The holes numbers in Fig. 7 are: 54 and 59 for *the top panel*; 107 for the middle panel; 43, 49, 55 and 57 for the bottom panel. *The right panels* show the same regions in Hα, with the dashed ellipses outlining the H I holes.

of each hole is the same as the average column density in its surroundings. The resulting distribution of missing masses is shown in Fig. 10e. The average H I mass missing from each holes is about 10^7 $M_\odot$. Adding over all holes gives a total missing H I mass of about 1.1×10^9 $M_\odot$, 15% of the total H I mass. The real missing H I mass is probably smaller, because the column densities in the surroundings of the holes are probably increased by the material swept up in the expansion of the shells.

3.3.4. Age

The ages of the holes are derived from their sizes using the average expansion velocity of 20 km s^{-1}. In Fig. 10c a histogram of the ages of the holes is shown. It shows a peak between 2 and 4×10^7 yr. The distribution looks similar to that of the diameters in Fig. 10, since we used the same expansion velocity for all holes. The presence of a peak would suggest a burst of hole formation, but more likely this shape is caused by selection effects. As already pointed out above, the small (young) holes may be missing because of lack of resolution of the observations and the old holes are harder to detect, because of shear and distortions due to the turbulent ISM.

There are almost no H I holes with bright H II complexes inside (see Fig. 8). If the holes were formed by stellar winds and SN explosions from OB associations, then the absence of these associations and H II complexes would imply that the holes were formed 2×10^7 yr ago or earlier (Heiles 1990).

We can also estimate an upper limit to the age of the holes taking a characteristic value for the velocity dispersion of the gas to calculate how long it would take to gradually fill them in. A value of 10 km s^{-1} for the dispersion results in ages between 4 and 8×10^7 yr.

Finally, we can calculate hole ages from their average ellipticity, assuming that they became elongated due to shear in the differentially rotating disk, by using the models from Palous et al. (1990). Figure 10d shows that most of the holes have an axis ratio between 0.7 and 1.0. The median value is 0.81. According to Palous et al. (1990), this corresponds to an age of about 4×10^7 yr. This is not too different from the other estimates.

The models by Palous et al. (1990) also predict that the position angle of the elongated holes is a function of time. We do not find this behaviour. The holes do, however, have a preferred alignment as can be seen from the histogram in Fig. 10f. Here we plot the distribution of pitch angles (angle between the major axis of the hole and the tangent to a circle at that galactic radius) which shows a sharp peak at 30°. This angle roughly coincides with the dominant pitch angle of the spiral structure.

There are other effects that could influence the ellipticity, besides shear. The shape of the holes is affected by the limited resolution of the data. The smallest holes appear rounder due to beam smearing. Furthermore, there are indications of substructure in the largest holes, which suggest that they may consist of a superposition of smaller holes. This would also affect the elongation. In addition, the structure of the ISM, in which the shells expand, may have an influence on the shape of the hole.

3.3.5. Kinetic energy

We estimate the energy needed to produce an H I hole using the formula by Heiles (1979). The estimated input energies in our sample are in the range of 10^{53}–10^{55} erg. These are high compared to the energies estimated for the holes in M 31 (Brinks & Bajaja 1986) and M 33 (Deul & den Hartog 1990). This is mostly due to the larger sizes of the holes in NGC 6946.

Silich et al. (1996) find in their simulations that an OB association giving an energy input of 10^{53} erg creates a superbubble with a diameter of about 1.3 kpc and a shell mass of 0.6×10^7 $M_\odot$ in 30 Myr. Our *average hole* has a size of 1.2 kpc, a missing mass of 10^7 $M_\odot$, an age of 30 Myr but an input energy of $\approx 1 \times 10^{54}$ erg. Timescales, sizes, and masses are in good agreement, but our input energy is large compared to those in the simulations. However, the uncertainty in the energy estimate is high, because it depends on ill-determined quantities such as the scale height of the gas disk and the assumed expansion velocities. If, for example, we assume a scale height of 250 pc instead of 200 pc and assume that we have overestimated the initial column density by 50%, the energies drop by a factor 2. Furthermore, if we follow Heiles (1979) and take the expansion velocity equal to the velocity dispersion of the surrounding ISM, which is about 10 km s^{-1} (instead of the assumed 20 km s^{-1}), the energy estimates would also become substantially lower.

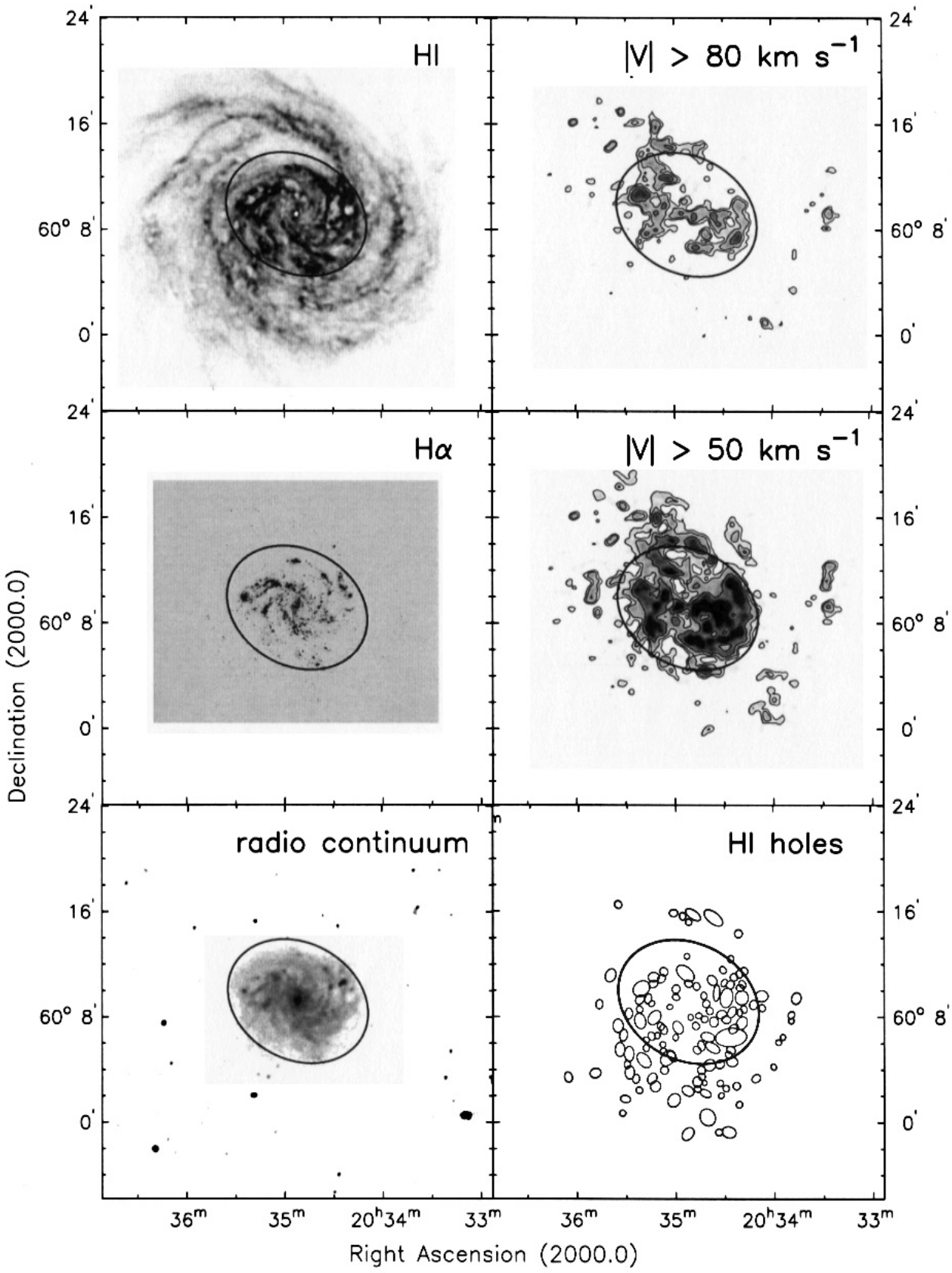

Fig. 9. *Top left*: the total H I distribution. *Middle left*: a deep H α image from Ferguson et al. (1998). *Top right*: the H I at velocities higher than ± 80 km s^{-1} with respect to the local galactic rotation at 22″ resolution. *Middle right*: the gas with deviations higher than 50 km s^{-1}. *Bottom right*: the catalogued holes indicated by ellipses. *Bottom left*: the 21-cm radio continuum. All panels are on the same scale. The ellipses outline the bright optical disk (D_{25}).

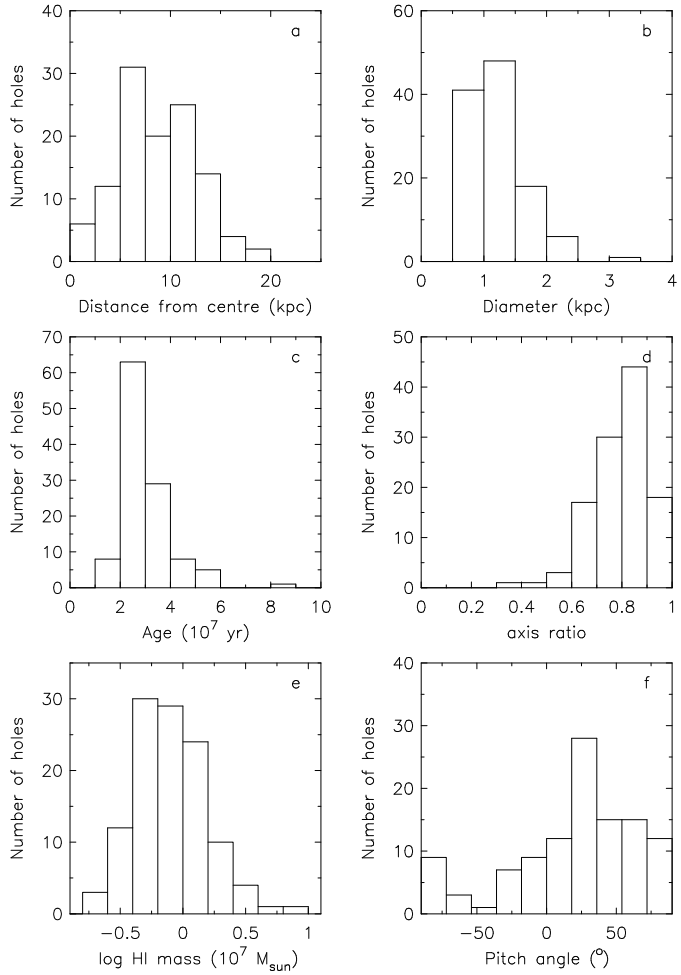

Fig. 10. Number distributions of the properties of the H I holes.

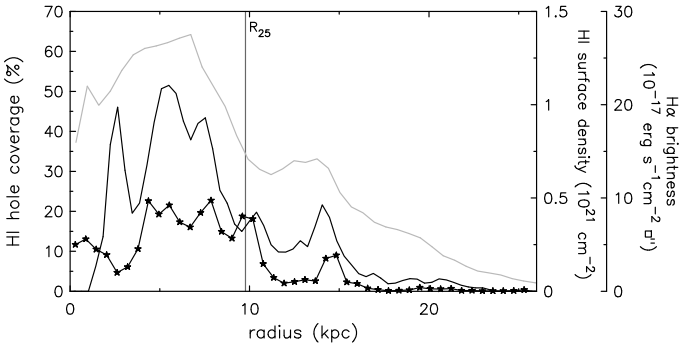

Fig. 11. The average covering factor of the H I holes as a function of the distance from the centre (black line) compared to the radial H I density distribution (grey line), and the H α surface brightness (connected stars).

3.4. High-velocity gas

Figure 12 shows six representative position-velocity plots extracted along the lines shown on the total H I map of NGC 6946 (top left). These *p-v* cuts show the regular, differentially rotating disk and a variety of features at anomalous velocities, some on the high-velocity side (as in cut 1), but most of them on the low-velocity side (as in cut 4), towards the systemic velocity. These are deviations (up to about 100 km s^{-1}) from circular motion (we refer to all of them as "high-velocity" clouds), which, in view of the low inclination of NGC 6946, must be in the vertical direction, showing gas leaving the disk or falling down onto it. In some cases (cuts 2 and 3) there seems to be an association with H I holes in the disk (Sect. 4.1). Most of the high-velocity gas is associated with the bright inner disk and seems to have, besides the obvious vertical motion, also an overall rotation lagging with respect to that of the disk (Sect. 3.4.2). Cuts 5 and 6 show the outer regions where the high-velocity gas is clearly associated with H I holes in the disk. This is related to the large-scale velocity wiggles visible in the velocity field (Fig. 2 and Sect. 4.4).

3.4.1. Derotation

In order to study the anomalous velocity gas component, we have separated it from the regularly rotating gas in the H I disk. We have defined all H I emission which differs more than 50 km s^{-1} from the local differential galactic rotation as *anomalous* H I or "high-velocity" H I. For each position (line of sight) we have defined the anomalous velocity $V_{\rm dev}$ as the velocity deviation from the velocity of the H I in the disk. The derotation has been effected by shifting each velocity profile in the data cube in such a way that all emission at velocities as represented in the velocity field (Fig. 2) appears in one single channel. This removes the systematic motion (disk rotation) and results in a data cube where the 3rd axis is $V_{\rm dev}$. In the derotated cube (Fig. 13), each channel shows H I at a given $V_{\rm dev}$ (see also Boulanger & Viallefond 1992). For reference, the total H I distribution is shown in the middle frame.

The top and bottom channels in Fig. 13 show that a significant amount of H I is present with $|V_{\rm dev}|$ larger than 50 km s^{-1} (see also Fig. 9). Since the H I velocity dispersion even in the central region does not exceed 12 km s^{-1}, these cannot be the wings of the Gaussian velocity distribution of the gas in the disk.

3.4.2. Distribution and kinematics

It is clear from Figs. 9 and 13 that most of the H I with $|V_{\rm dev}| >$ 50 km s^{-1} is seen in the direction of the bright optical disk (outlined at R_{25} by the ellipse).

The high-velocity emission is not distributed symmetrically with respect to the centre of NGC 6946. The gas with negative $V_{\rm dev}$ is more extended to the south-west, while the gas with positive velocities shows the opposite. In a *p-v* diagram of the original (non-derotated) data this anomalous gas is thus seen mainly on the lower rotational side of the cold disk emission (Fig. 14) as a *beard* (Sancisi et al. 2001). This is similar to what is observed in more inclined galaxies such as NGC 2403 (Fraternali et al. 2001) and NGC 4559 (Barbieri et al. 2005). The *beard* in NGC 2403 has been interpreted as a manifestation of a lagging H I halo. There is, however, an important difference: in NGC 6946, emission is also seen at the high rotational velocity side. The velocities of this gas can not be explained as rotation (see Sect. 4.3).

In addition, there is H I at so-called *forbidden* velocities, i.e. apparently counter-rotating. An example can be seen in Fig. 14 (right panel) in the quadrant left of the centre and at positive velocities. Figure 14 also shows that the high-velocity H I has a clumpy structure at high resolution.

Figure 15 shows the velocity distribution of the derotated H I emission after integrating along the minor axis of the galaxy. The vertical dashed lines mark the boundary of the optically bright disk. Also shown is the H α emission (data from Ferguson et al. 1998) after integration in the same direction (profile at the

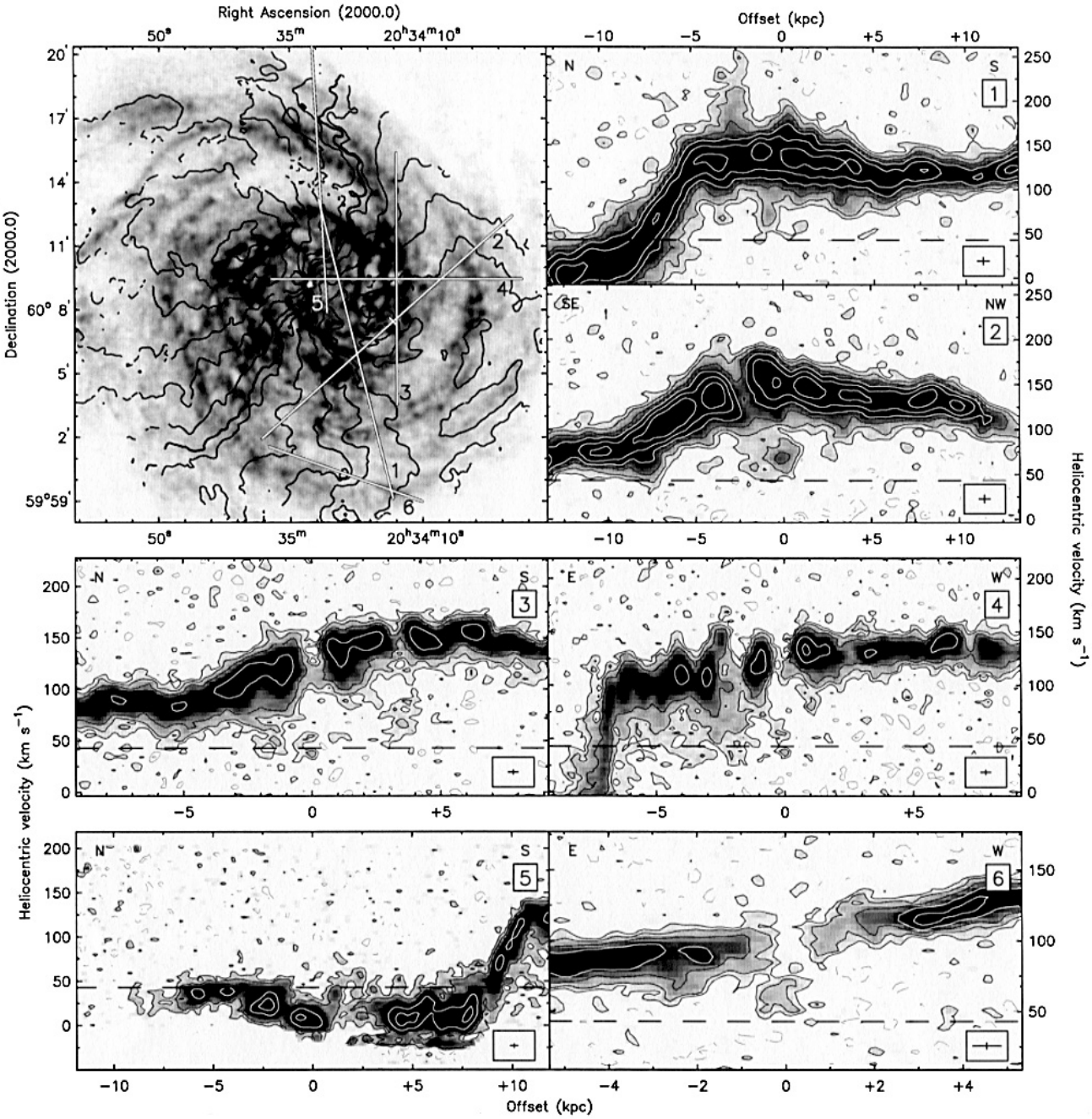

Fig. 12. Six position-velocity plots showing high-velocity features and gas at peculiar velocities in NGC 6946. *The top left panel* shows the total H I map and velocity field with overlaid the locations of the cuts. Contours are at –0.75, –0.4, 0.4 (1.5σ), 0.75, 1.5, 3, 6, 12, and 24 mJy beam^{-1} for *the two top right panels* and *the bottom right panel* (22″ resolution) and –1.3, –0.66, –0.33, 0.33 (1.5σ), 0.66, 1.3, 2.6, 5.2, and 10 mJy beam^{-1} for the other panels (13″ resolution). The resolution is shown in the bottom right corners. The horizontal gray dashed line shows V_{sys}.

bottom of Fig. 15). This diagram illustrates the overall spatial-velocity structure of the H I after derotation. It clearly shows that: i) the high-velocity H I tails and the H α emission are highly concentrated in the direction of the bright inner disk of NGC 6946; ii) there is a remarkable position-velocity skewness in the distribution of the high-velocity H I. The origin of this skewness can be understood in this way: the *p-v* diagram in Fig. 14 shows that there is more gas below than above the rotation velocities. This is the beard (e.g. Fraternali et al. 2001). In the derotation, using the rotation curve of the disk, obviously the disk emission moves to velocities around 0 km s^{-1}, while the beard gas (which has velocities lower than rotation) is shifted to negative velocities. This is precisely what is observed in Fig. 16, on the right side (receding side of the galaxy). A similar shift in the opposite sense (towards positive velocities) occurs on the left side of the figure (approaching side of the galaxy). This gas, in our view, is located in the halo of NGC 6946 and the skewness is the manifestation of its lagging rotation (see Sect. 4.3).

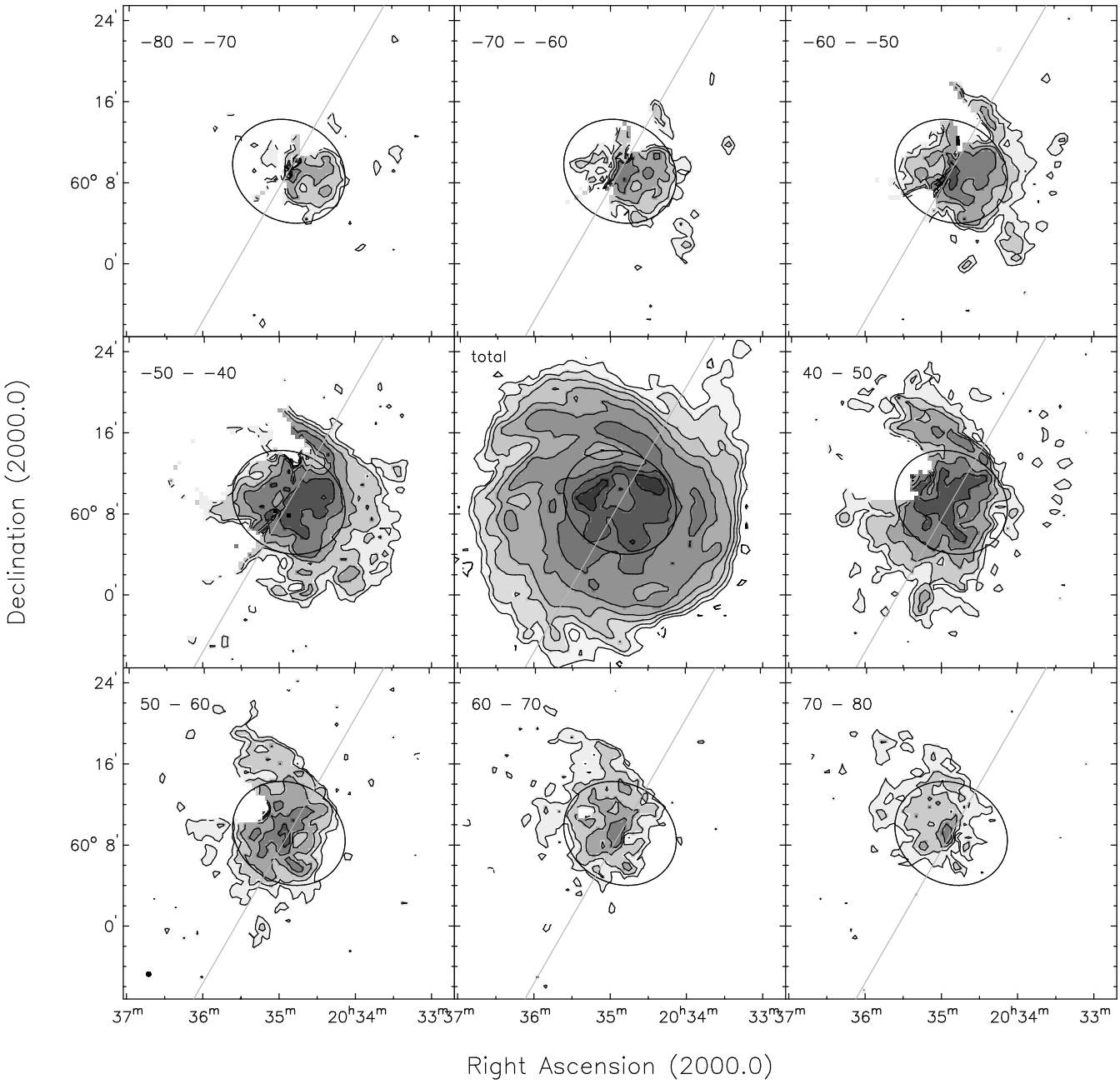

Fig. 13. Channel images at 64″ resolution after derotation. The channel separation and width are about 10 km s^{-1}. In *the top-left corner of each panel*, the velocity range relative to the disk rotation is shown. Contours are at −2.56, −1.28, 1.28 (1.5σ), 2.56, 5.12, 10.2, 20.4, and 40.8 mJy beam^{-1}. *The central panel* shows the total H I for comparison. Contours are plotted for 0.25, 0.5, 1, 2, 4, 8, 12, and 16×10^{20} cm^{-2}. The grey line shows the kinematic minor axis. The ellipse outlines the region inside R_{25}. The beam size is indicated in the bottom-left corner of the bottom left panel.

4. Discussion

4.1. Holes and star formation

The most likely mechanism for producing holes in the H I distribution is the expansion (and blow-up) of superbubbles created by multiple supernova explosions around large stellar clusters. In some of the nearest galaxies (M 31, M 33, SMC), where individual OB associations can be detected, a correlation is found between these associations and small (<200–300 pc) H I holes (Brinks & Bajaja 1986; Deul & den Hartog 1990; Hatzidimitriou et al. 2005). For large holes and shells no correlation is seen. At their interior, the H I holes of NGC 6946 (all larger than ~800 pc) generally show no bright optical/UV emission, no radio continuum (Fig. 9) and no Far Infrared (FIR) emission (Contursi et al. 2002). This suggests that these holes are really devoid of gas and dust and star formation.

During their formation, the interiors of the bubbles are thought to contain hot gas, heated by the SN explosions and stellar winds, that should be observable in X-rays. Chandra observations of NGC 6946 (Schlegel et al. 2003) show diffuse X-ray emission toward the star forming regions (traced by the largest H II complexes, see their Fig. 10) but only a few regions with X-ray emission coincide with H I holes in our sample.

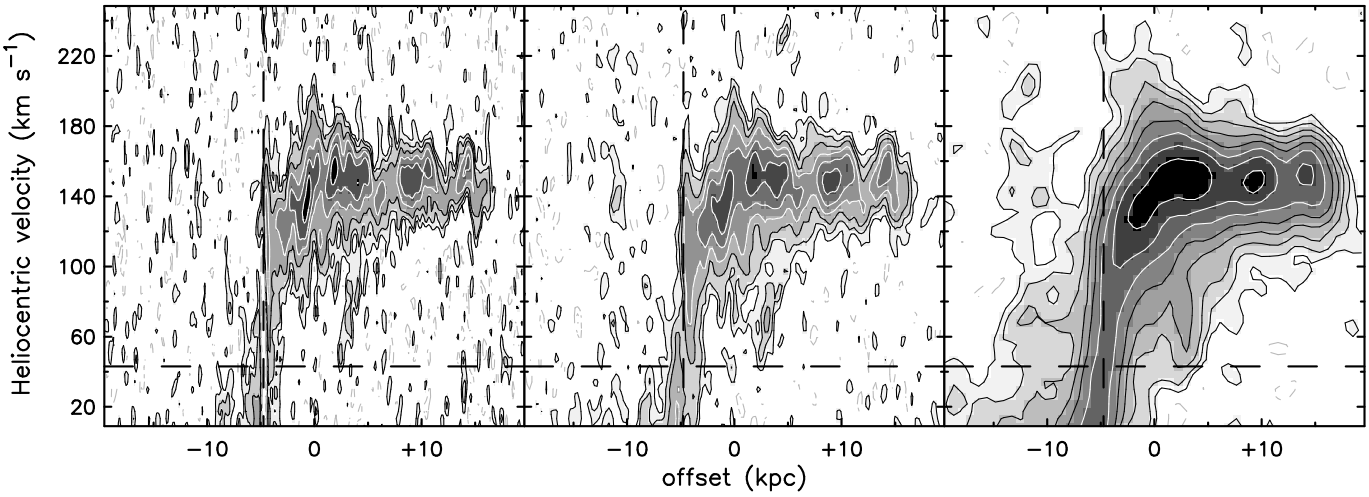

Fig. 14. Position-velocity diagram near the major axis. *The left panel* is at 13″ resolution, the middle at 22″, and *the right panel* at 64″ resolution. In all panels the contours are at -3σ, -1.5σ, 1.5σ, 3σ, 6σ, 12σ, 24σ, and 48σ. The rms noise values are respectively 0.15, 0.25, and 0.43 mJy beam^{-1}. The vertical dashed line indicates the centre of the galaxy, the horizontal dashed line the systemic velocity.

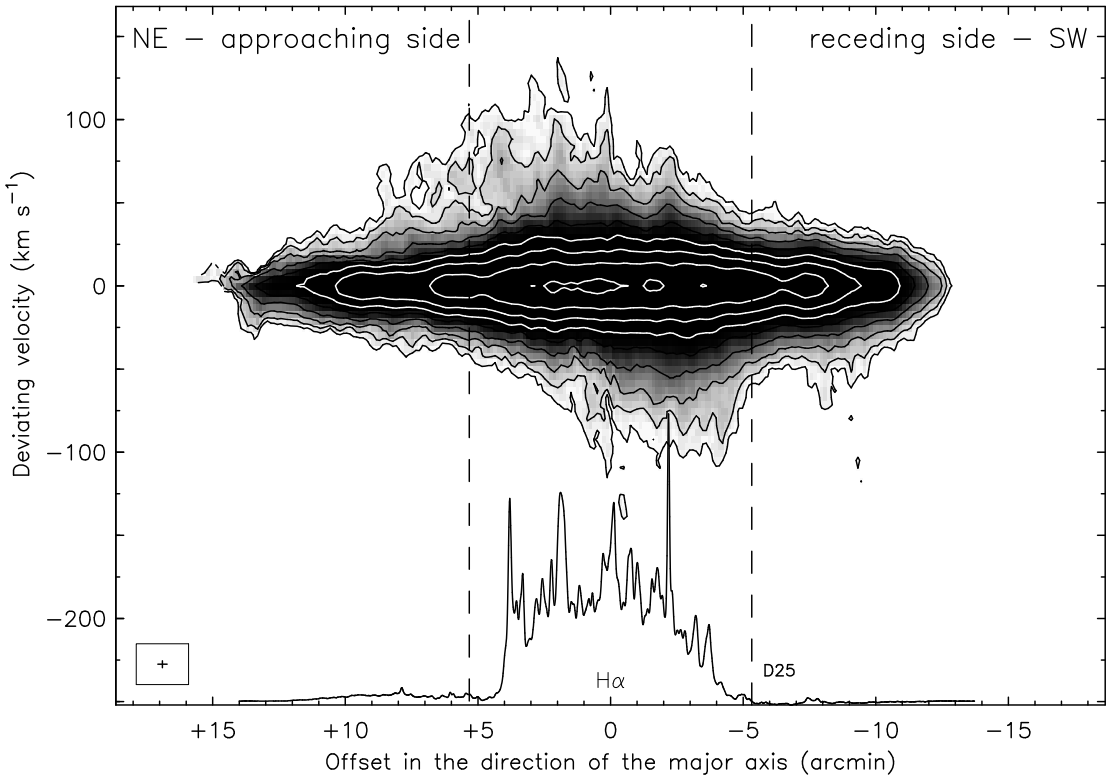

Fig. 15. A total H I *pv* diagram for NGC 6946 parallel to the major axis after strip integration of the derotated H I emission along the minor axis. The bottom profile shows the H α emission also integrated along the minor axis. The vertical dashed lines indicate the D_{25} of NGC 6946. Contour values are 1, 2, 4, 8, ..., 256 (arbitrary units).

Those holes are also the few cases that coincide with bright star clusters.

In Fig. 16 we show a close-up of the hole labelled as 51 in Fig. 7. This is a spherical H I hole with a diameter of about 800 pc, among the smallest in our sample. In the same direction an H α bubble is detected, which seems to fill the H I cavity (Fig. 16, top right). At the western rim, one or more OB associations are seen surrounded by a bright H II complex. The H I kinematics shows a two-sided spur which seems to be centred on the H II complex and can be interpreted as an outflow (Fig. 16, bottom panels). There is X-ray emission coinciding with the H α bubble, which indicates a hot interior. The presence of the H α bubble, the X-ray emission, as well as the small size and spherical shape indicate that the H I hole is still relatively young. We estimate an age of 1.9×10^7 yr.

The most extended region where stellar activity seems to coincide with a group of H I holes is the north-eastern spiral arm, about 6 kpc from the nucleus. In optical this spiral arm seems

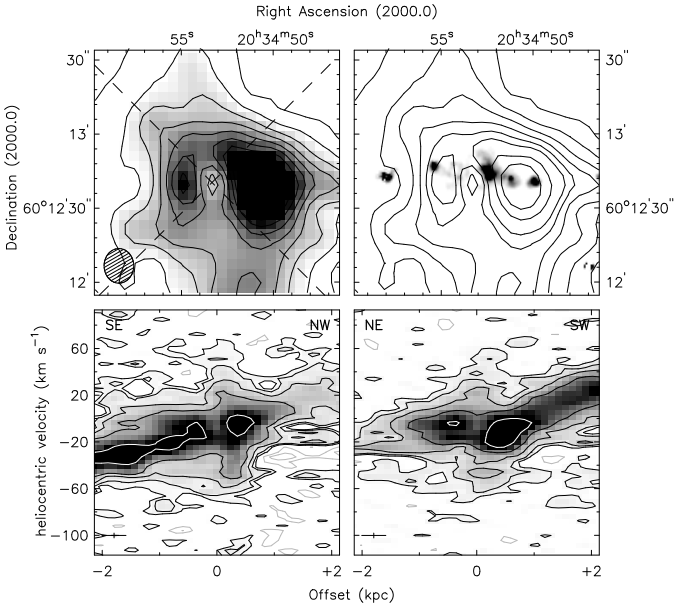

Fig. 16. Example of a hole coinciding with an H α bubble and H I outflow next to it. *The top left panel* shows the channel at 8 km s^{-1} (hel. velocity) in which the hole is best seen (greyscale). The beam is indicated by the shaded ellipse. *The top right panel* shows the H α emission in greyscale. *The bottom panels* are *pv*-diagrams along the dashed lines in the top left panel. The crosses indicate the resolution.

thicker than the others and in H I it appears split by a group of H I holes, the largest of which is No. 20 (see Fig. 7). Inside the holes, large clusters of blue stars are seen. The high contrast and colour difference with its surroundings could also be the effect of extinction. Diffuse soft X-rays are detected over the entire spiral arm as well as diffuse H α emission (Ferguson et al. 1998). Figure 9 shows that there is high-velocity gas in the direction of the holes.

Expanding shells are expected to compress the surrounding ISM enhancing gravitational collapse and triggering new star formation. In NGC 6946 there is strong evidence for this taking place. Figure 8 shows clear examples of bright H II regions in the rims of the H I shells. Note that they belong to very different environments: a crowded region close to the nucleus (upper panel), the large H I hole No. 107 in the western spiral arm (middle panel) and the northern spiral arm beyond R_{25} (bottom panel).

To test the hypothesis that H I holes are formed by explosion of a large number of supernovae we can compare the energies associated to the two processes. For the star-formation rate of NGC 6946 we take the estimate from FIR and C^+ emission by Sauty et al. (1998), which gives 4 $M_\odot$ yr^{-1}. This corresponds to a SN rate of about 4×10^{-2} yr^{-1} and a full energy input of $\sim 6 \times 10^{55}$ erg Myr^{-1}, having included also a contribution from stellar winds. On the other side of the balance, the energy needed to create the holes in NGC 6946 is 1.8×10^{56} erg (using the energy formula by Heiles 1979). Given that the typical lifetime for the H I holes is of about 30 Myr, the required energy input becomes 6×10^{54} erg Myr^{-1}, about 10% of the available energy from SNe.

Although the energy budgets seem roughly right for the stellar feedback to produce the holes, it is still a puzzle that we observe many H I holes without progenitor remnants. If a hole was formed by 1000 SNe, an over-density of the lower mass stars that formed together with the massive SNe-progenitors would be expected: 6000 upper main sequence stars (late B, A, and F) should remain after 10^8 yr (Rhode et al. 1999). After that time, the clusters will not have dispersed significantly and they should be observable as blue point sources inside the holes. Possible explanations are that the ages of the holes have been largely underestimated or that the holes are formed by the combined effect of several small clusters which would lead to a much more diffuse emission.

Alternatively, the holes can be formed by collisions of gas clouds with the H I disk of the galaxy (Tenorio-Tagle et al. 1986, 1987; Vorobyov & Basu 2005). In NGC 6946 there are some indications that this may occasionally be happening. Figure 12 (bottom right) shows a *p-v* plot from the outer parts of the H I disk. Large deviations from normal rotation are detected in this area as one can see also from the velocity field in Fig. 2. The high-velocity gas, visible in Fig. 12, is shifted by about 50 km s^{-1} with respect to the surrounding gas and follows the kinematical distortion of the spiral arm wiggles. It is detected in an inter-arm region where star formation is scarce or absent, which makes the possibility of a stellar origin quite unlikely. A cloud collision in this area may be advocated also to explain the prominent spiral arms in the outer disk (see also Sancisi et al. 2008).

4.2. Holes and high-velocity gas

Most of the high-velocity gas complexes are found in regions of high hole density (Fig. 9) predominantly within the star forming, optical disk as outlined by R_{25}. However, the asymmetric distribution of the holes to the south is not reflected in the distribution of high-velocity H I (Fig. 9, middle-right panel) showing that the connection between holes and the high-velocity is not straightforward.

On the small scale there are only a few cases of clear connections between high-velocity gas and holes. A possible example is given by cuts Nos. 2 and 3 in Fig. 12 where a large high-velocity cloud (mass 2.5×10^6 $M_\odot$) is detected shifted by about 80 km s^{-1} in the direction of the hole No. 108. Smaller complexes are also observed in connection with the remarkable hole No. 107 (cuts Nos. 3 and 4).

The lack of an obvious connection with the holes can, in some cases, be explained by taking into account the different kinematics between disk and halo. According to galactic fountain models (Collins et al. 2002; Fraternali & Binney 2006), gas can stay in the halo for about half a rotation period (few 10^7–10^8 yr). Since the halo is rotating more slowly than the cold disk, this time is long enough for the gas to drift a few kpc away from its origin in the disk.

If the high-velocity gas is produced by the blow-out (into the halo) of the superbubbles that produce the holes in disk, the missing mass from the holes should be comparable with the mass of gas at high velocities. The H I mass missing from the holes is 1.1×10^9 $M_\odot$, while the amount of H I with $|V_{\rm dev}| > 50$ km s^{-1} is 2.9×10^8 $M_\odot$. The former may be overestimated because of the reasons described in Sect. 3.3.3. The latter is certainly underestimated because it does not take into account the hydrogen that has been ionised and, especially, the large fraction of H I with smaller $|V_{\rm dev}|$. In fact, if we lower the cut in velocity to $|V_{\rm dev}| > 40$ km s^{-1}, the total amount of high-velocity H I becomes of order 10^9 $M_\odot$. We conclude that the missing mass from the holes and the mass of high-velocity H I are comparable, supporting the hypothesis that the two phenomena are related.

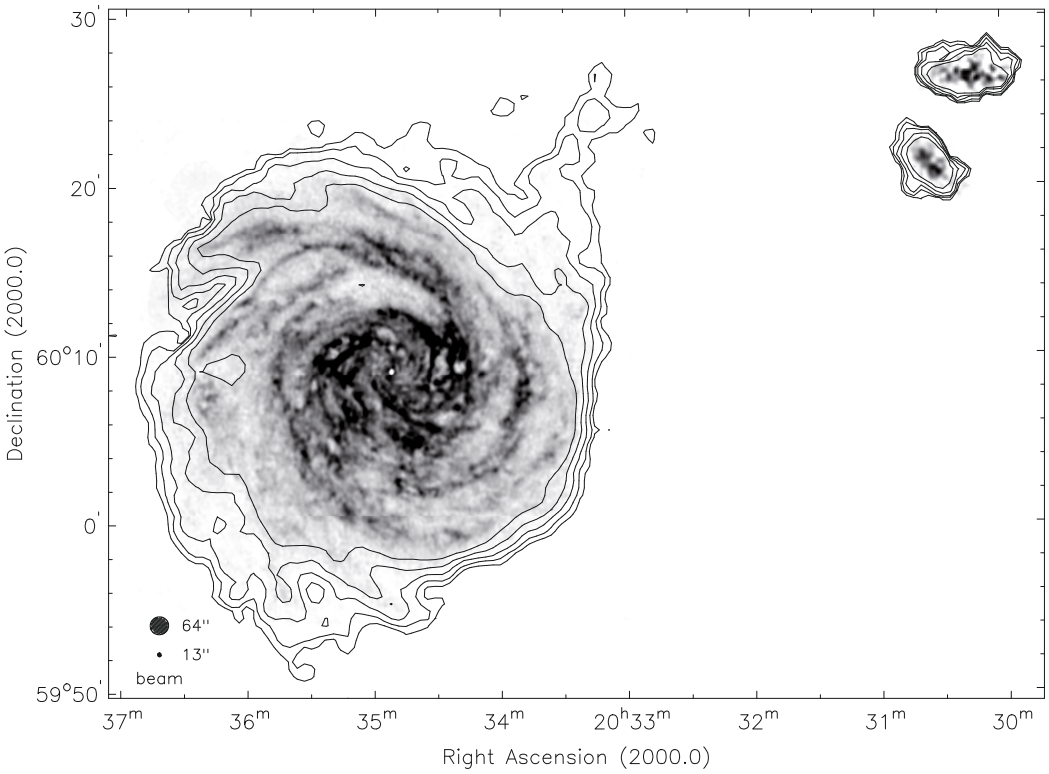

Fig. 17. Total H I map at 13″ and 64″ resolution of NGC 6946 and two companions. The map has been corrected for primary beam attenuation. The greyscale shows the high resolution. The contours (1.25, 2.5, 5, 10, and 20×10^{19} cm^{-2}) show the 64″ low resolution H I distribution. The highest emission contours have been left out. The sizes of the beams for both resolutions are shown in the lower left corner.

4.3. Extra-planar gas

Where is the high-velocity gas located? Is it extra-planar? The observations have shown that: 1) the high-velocity gas is mainly seen in the direction of the inner, optically bright disk (Figs. 9 and 14); 2) there is more gas with lower than with higher velocities as compared to the local disk rotation, 2.4×10^8 $M_\odot$vs. 0.5×10^8 $M_\odot$(Figs. 14 and 16). This shows up as a striking asymmetry/skewness in Fig. 16.

Result No. 1 points to a fountain origin of the high velocity H I and, considering the low inclination of the galaxy, the motion is probably dominated by vertical out- and in-flows. In this case one would expect, contrary to result No. 2, symmetry (i.e. equal amplitudes and equal amounts of gas) between the lower and the higher velocities. Result No. 2 resembles, instead, a so-called *beard* (Sancisi et al. 2001) and leads us to think that the high-velocity gas (or a large fraction of it) is extra-planar and rotates more slowly than the gas in the disk. Also NGC 6946 seems, therefore, to be surrounded by a lagging halo of cold gas as NGC 891 (Swaters et al. 1997; Oosterloo et al. 2007) and NGC 2403 (Schaap et al. 2000; Fraternali et al. 2001). We do not derive the amplitude of the lag but it is clear that, for the effect to be so striking (as in Fig. 16), the lag in rotation must be quite pronounced, as found in NGC 891 (Oosterloo et al. 2007). It is not known what is causing such a large rotational gradient. It seems unlikely that galactic fountain models, by themselves, can explain it (Fraternali & Binney 2006; Heald et al. 2006). For NGC 891 and NGC 2403 it has been suggested that the gradient is the result of interactions between the fountain gas and accreting ambient gas carrying low angular momentum (Fraternali & Binney 2008).

4.4. Interactions and accretion

Earlier observations report "no signatures of interactions in the NGC 6946 system" (Pisano & Wilcots 2000). We have detected, however, a plume-like structure at the north-western edge of the disk (Fig. 17), that may be related to a recent interaction. This plume is a very faint feature that can be revealed only with high sensitivity and at low resolution. That is probably why it was missed in previous observations.

The velocity of the plume is in the same range as the two companion galaxies that happen to be on the same side of NGC 6946. Their projected distances from the centre of NGC 6946 are about 33 and 37 kpc respectively. We did not find any emission in between them and the plume. However, far away from the pointing centre the sensitivity of our observations drops rapidly because of the attenuation by the WSRT primary beam. At the position of the companions, the sensitivity is only 2% of that at the centre of the field. To overcome this problem new observations were made with the telescope pointing in the direction between NGC 6946 and its companions; but no connection was found between the plume and the companions. The limiting column density is about 5×10^{19} cm^{-2}.

A lower limit for the mass of the plume is about 7.5×10^7 $M_\odot$. This is of the order of the gas mass of the companions (1.2×10^8 $M_\odot$ and 8.8×10^7 $M_\odot$). It is possible that we witness the aftermath of the accretion of a third companion galaxy. In deep optical images no emission is visible in the direction of the plume. If, however, the companion has been tidally disrupted, the surface density of stars can be well below the detection limit. The plume may also have formed out of an intergalactic H I complex which contains no stars. Alternatively, the plume is

originating from the H I disk of NGC 6946, pulled out from the galaxy by tidal interaction, which would also explain the similarity in velocity with the disk of NGC 6946 at that position.

There are other indications that NGC 6946 may have undergone tidal interactions in the recent past:

1. its lopsidedness. Both its H I and stellar distribution are somewhat asymmetric. Also its kinematics is lopsided in the outer parts: the rotation curves which have been derived separately for the approaching and for the receding side (Fig. 4) differ at large radii (one remains flat while the other is declining). It has been suggested that lopsidedness can be produced by recent or ongoing accretion (Zaritsky & Rix 1997; Bournaud et al. 2005);
2. the sharp edge of the H I disk on the south-west side. Such edges are seen in galaxies that undergo tidal interaction, e.g. M 51 (Rots et al. 1990) and M 81 (Yun et al. 1994). Ram pressure seems unlikely here, in the absence of a dense cluster medium;
3. the peculiar kinematical structure (H I cavity and high-velocity) in the outer disk, outside the star forming regions (Fig. 12, cut 6). This shows up as a strong wiggle in the velocity field which extends for 10–15 kpc following the prominent outer spiral arm (Figs. 2 and 12). If the observed structure has been caused by a gas complex falling in and penetrating the disk, this must have occurred quite recently, probably not more than a few times 10^7 yr, as we still see the high-velocity H I located well in front of the hole (see also Sect. 4.1).

5. Summary and conclusions

We have reported 21-cm line observations, among the deepest for a spiral to date, of the low-inclination galaxy NGC 6946. We have found:

1) A large number of holes in the HI disk. Sizes are up to 3 kpc diametre. They are mostly located within the bright optical disk and preferentially in regions of high H I column density and star formation. Their ages are in the range of 1 to 6×10^7 yr. Some of them have H II regions at their rims.
2) Widespread, clumpy high-velocity H I. The velocities are up to about 100 km s^{-1} (for the faintest features at the detection limit). Most of the high-velocity gas is seen in the direction of the inner bright optical disk. It has a rotational component following the disk rotation but lagging behind it. There is also some H I at forbidden velocities. The total mass of the gas with $|V_{\rm dev}| > 50$ km s^{-1} is 2.9×10^8 $M_\odot$, 4% of the total H I mass.
3) A large H I outer plume, sharp outer edges, and a lopsided structure and kinematics. In the outer parts there are also pronounced velocity wiggles and associated H I cavities.
4) H I disk velocity dispersion reaching maximum values of 12–13 km s^{-1} inside R_{25} and decreasing (linearly) down to 6 km s^{-1} in the outer parts.

We conclude that:

1) The high-velocity H I is extra-planar gas which rotates more slowly than the disk. This has the same properties as the H I halos found in nearby spiral galaxies such as NGC 891, NGC 2403 and also the Milky Way (IVCs and HVCs).
2) Most of this extra-planar H I is fountain gas which originates from the regions of star formation in the bright inner disk and is probably related to the presence of the numerous H I holes.
3) There is evidence, mainly in the outer parts of NGC 6946, pointing to recent tidal encounters and minor mergers.

Acknowledgements. We are grateful to Jacqueline van Gorkom for valuable discussions and comments, and we thank Annette Ferguson for kindly providing the deep H α data for NGC 6946.
The Westerbork Synthesis Radio Telescope is operated by ASTRON (the Netherlands Institute for Radio Astronomy) with financial support from the Netherlands Foundation for the Advancement of Pure Research (N.W.O).

References

Barbieri, C. V., Fraternali, F., Oosterloo, T., et al. 2005, A&A, 439, 947
Battaglia, G., Fraternali, F., Oosterloo, T., & Sancisi, R. 2006, A&A, 447, 49
Begeman, K. G. 1989, A&A, 223, 47
Boomsma, R. 2007, Ph.D. Thesis, Kapteyn Astronomical Institute, University of Groningen
Boulanger, F., & Viallefond, F. 1992, A&A, 266, 37
Bournaud, F., Combes, F., Jog, C. J., & Puerari, I. 2005, A&A, 438, 507
Bregman, J. N. 1980, ApJ, 236, 577
Briggs, D. S. 1995, in BAAS, 1444
Brinks, E., & Bajaja, E. 1986, A&A, 169, 14
Carignan, C., Charbonneau, P., Boulanger, F., & Viallefond, F. 1990, A&A, 234, 43
Collins, J. A., Benjamin, R. A., & Rand, R. J. 2002, ApJ, 578, 98
Contursi, A., Kaufman, M. J., Helou, G., et al. 2002, AJ, 124, 751
de Avillez, M. A., & Berry, D. L. 2001, MNRAS, 328, 708
de Vaucouleurs, G., de Vaucouleurs, A., & Corwin, J. R. 1976, in Second reference catalogue of bright galaxies (Austin: University of Texas, Press)
Degioia-Eastwood, K., Grasdalen, G. L., Strom, S. E., & Strom, K. M. 1984, ApJ, 278, 564
Deul, E. R., & den Hartog, R. H. 1990, A&A, 229, 362
Ferguson, A. M. N., Wyse, R. F. G., Gallagher, J. S., & Hunter, D. A. 1998, ApJ, 506, L19
Fraternali, F., & Binney, J. J. 2006, MNRAS, 366, 449
Fraternali, F., & Binney, J. 2008, ArXiv e-prints, 802
Fraternali, F., Oosterloo, T., Sancisi, R., & van Moorsel, G. 2001, ApJ, 562, L47
Gordon, K. J., Remage, N. H., & Roberts, M. S. 1968, ApJ, 154, 845
Hatzidimitriou, D., Stanimirovic, S., Maragoudaki, F., et al. 2005, MNRAS, 360, 1171
Heald, G. H., Rand, R. J., Benjamin, R. A., & Bershady, M. A. 2006, ApJ, 647, 1018
Heiles, C. 1979, ApJ, 229, 533
Heiles, C. 1990, ApJ, 354, 483
Kamphuis, J., & Sancisi, R. 1993, A&A, 273, L31
Kamphuis, J. J. 1993, Ph.D. Thesis, University of Groningen
Karachentsev, I. D., Sharina, M. E., & Huchtmeier, W. K. 2000, A&A, 362, 544
Kim, S., Dopita, M. A., Staveley-Smith, L., & Bessell, M. S. 1999, AJ, 118, 2797
Mac Low, M.-M., & McCray, R. 1988, ApJ, 324, 776
McCray, R., & Kafatos, M. 1987, ApJ, 317, 190
Oosterloo, T., Fraternali, F., & Sancisi, R. 2007, AJ, 134, 1019
Palous, J., Franco, J., & Tenorio-Tagle, G. 1990, A&A, 227, 175
Pisano, D. J., & Wilcots, E. M. 2000, MNRAS, 319, 821
Puche, D., Westpfahl, D., Brinks, E., & Roy, J.-R. 1992, AJ, 103, 1841
Rhode, K. L., Salzer, J. J., Westpfahl, D. J., & Radice, L. A. 1999, AJ, 118, 323
Rogstad, D. H., Shostak, G. S., & Rots, A. H. 1973, A&A, 22, 111
Rots, A. H., Bosma, A., van der Hulst, J. M., Athanassoula, E., & Crane, P. C. 1990, AJ, 100, 387
Sancisi, R., Fraternali, F., Oosterloo, T., & van Moorsel, G. 2001, in Gas and Galaxy Evolution, ed. J. E. Hibbard, M. Rupen, & J. H. van Gorkom, ASP Conf. Ser., 240, 241
Sancisi, R., Fraternali, F., Oosterloo, T., & van der Hulst, J. M. 2008, ArXiv e-prints, 803
Sault, R. J., Teuben, P. J., & Wright, M. C. H. 1995, in Astronomical Data Analysis Software and Systems IV, ed. R. A. Shaw, H. E. Payne, & J. J. E. Hayes, ASP Conf. Ser., 77, 433
Sauty, S., Gerin, M., & Casoli, F. 1998, A&A, 339, 19
Schaap, W. E., Sancisi, R., & Swaters, R. A. 2000, A&A, 356, L49
Schlegel, E. M., Holt, S. S., & Petre, R. 2003, ApJ, 598, 982
Shapiro, P. R., & Field, G. B. 1976, ApJ, 205, 762
Silich, S. A., Franco, J., Palous, J., & Tenorio-Tagle, G. 1996, ApJ, 468, 722
Stanimirovic, S., Staveley-Smith, L., Dickey, J. M., Sault, R. J., & Snowden, S. L. 1999, MNRAS, 302, 417
Swaters, R. A. 1999, Ph.D. Thesis, Rijksuniversiteit Groningen

Swaters, R. A., Sancisi, R., & van der Hulst, J. M. 1997, ApJ, 491, 140
Tacconi, L. J., & Young, J. S. 1986, ApJ, 308, 600
Tenorio-Tagle, G., & Bodenheimer, P. 1988, ARA&A, 26, 145
Tenorio-Tagle, G., Bodenheimer, P., Rozyczka, M., & Franco, J. 1986, A&A, 170, 107
Tenorio-Tagle, G., Franco, J., Bodenheimer, P., & Rozyczka, M. 1987, A&A, 179, 219
Thilker, D. A., Braun, R., & Walterbos, R. M. 1998, A&A, 332, 429
Tomisaka, K., & Ikeuchi, S. 1986, PASJ, 38, 697
van der Hulst, J. M., Terlouw, J. P., Begeman, K. G., Zwitser, W., & Roelfsema, P. R. 1992, in Astronomical Data Analysis Software and Systems I, ed. D. M. Worrall, C. Biemesderfer, & J. Barnes, ASP Conf. Ser., 25, 131
van der Hulst, T., & Sancisi, R. 1988, AJ, 95, 1354
van Dyk, S. D., Hyman, S. D., Sramek, R. A., & Weiler, K. W. 1994, IAU Circ., 6045, 2
van Woerden, H., & Wakker, B. P. 2004, in High Velocity Clouds, ed. H. van Woerden, B. P. Wakker, U. J. Schwarz, & K. S. de Boer (Dordrech: Kluwer Academic Publishers), Astrophys. Space Sci. Library, 312, 195
Vogelaar, M. G. R., & Terlouw, J. P. 2001, in Astronomical Data Analysis Software and Systems X, ed. F. R. Harnden, Jr., F. A. Primini, & H. E. Payne, ASP Conf. Ser., 238, 358
Vorobyov, E. I., & Basu, S. 2005, A&A, 431, 451
Wakker, B. P., & Schwarz, U. J. 1988, A&A, 200, 312
Wakker, B. P., & van Woerden, H. 1997, ARA&A, 35, 217
Wakker, B. P., York, D. G., Howk, J. C., et al. 2007, ApJ, 670, L113
Wakker, B. P., York, D. G., Wilhelm, R., et al. 2008, ApJ, 672, 298
Walter, F., & Brinks, E. 1999, AJ, 118, 273
Wilcots, E. M., & Miller, B. W. 1998, AJ, 116, 2363
Yun, M. S., Ho, P. T. P., & Lo, K. Y. 1994, Nature, 372, 530
Zaritsky, D., & Rix, H.-W. 1997, ApJ, 477, 118